Article

Journal of
Nanoscience and Nanotechnology
Vol. 14, 8952–8956, 2014
www.aspbs.com/jnn

Fabrication and Characteristics of Hexagonal Zn Nanowires Prepared by Heating a Mixture of Zn and Graphite Powders

Hyoun Woo Kim[1,*], Yong Jung Kwon[1], Hong Yeon Cho[1], Han Gil Na[1], and Chongmu Lee[2]

[1]Division of Materials Science and Engineering, Hanyang University, Seoul 133-791, Republic of Korea
[2]School of Materials Science and Engineering, Inha University, Incheon 402-751, Republic of Korea

We report the fabrication of thin (< 100 nm) hexagonal Zn nanowires in a conventional reactor, by heating a mixture of Zn and graphite powders. By material characterization, the products were identified as one-dimensional nanowires of serpent-like morphology with a hexagonal Zn phase. The main growth mechanism of the Zn nanowires was proposed to be a vapor-solid process, which was corroborated by the absence of any tip catalyst. Raman spectra of the Zn nanowires exhibited a prominent peak at around 570 cm^{-1}. X-ray photoelectron spectroscopy revealed that the surface of the Zn nanowires was clearly oxygen-deficient in comparison to that of ZnO nanowires. Photoluminescence analysis indicated that the Zn nanowires exhibited emission bands centered at 1.6, 2.0, 2.4, 3.0, and 3.3 eV, respectively.

Keywords: Zn, Nanowires, Evaporation.

1. INTRODUCTION

With the development of one-dimensional (1D) nanomaterials,[1–6] 1D nanostructures of various metals have been intensively studied, due to their importance not only in fundamental research but also in technological applications.[7–10] Among the candidate metals for 1D nanostructures, zinc (Zn) is one of the most useful transition metals. Metallic Zn is an important conventional type-I superconductor. Its traditional applications include corrosion-resistant Zn plating of iron (i.e., galvanizing), batteries, small non-structural castings, etc. Furthermore, a variety of Zn compounds or alloys have been formed for diverse applications. Although study of the fabrication and characteristics of Zn 1D nanomaterials is urgently required, only a few articles have been reported.

Chang et al. prepared Zn nanowires by electrochemical anodization.[11] Vivekchand et al. utilized a nebulized spray pyrolysis technique to synthesize wool-like Zn nanowires by decomposition of Zn acetates at temperatures of 800–1000 °C.[12] Kast et al. prepared Zn nanowires of two different morphologies by the cold-wall physical vapor deposition method.[13] In addition, template synthesis by electrochemical deposition has been carried out to prepare Zn nanowires.[14, 15] For example, Wang et al. reported the fabrication of Zn nanowires by electrodeposition into the holes of porous anodic alumina membrane.[14] Wang et al. instead used polycarbonate templates.[15]

In the present work, to investigate the feasibility of a low-cost, simple, and low-temperature process, we have fabricated single crystalline Zn nanowires by simple heating of a mixture of Zn and graphite powders. This method can provide an efficient way to apply Zn nanowires to future ultra large scale integration devices. We have suggested the growth mechanism of these Zn nanowires in the present work. In addition, for the first time we obtained Raman and X-ray Photoelectron Spectroscopy (XPS) spectra of Zn nanowires. In particular, XPS spectra confirmed that the surface of the Zn nanowires is comprised of ZnO_x structures.

2. EXPERIMENTAL DETAILS

Zn nanowires were synthesized in a quartz tube by directly heating a mixture of Zn and graphite powders. In the combined carrier gas of Ar and O_2 with a constant total

*Author to whom correspondence should be addressed.

1533-4880/2014/14/8952/005 doi:10.1166/jnn.2014.10060

pressure of 1 Torr, the percentage of the O_2 partial pressure was set to about 3%. The growth temperature was set to 900 °C for 1 h. The total weight of the powder mixture was kept to 0.04 g, and the molar ratio of Zn powder was set to 0.5. Herein, the molar ratio of Zn powder is defined as the moles of Zn powders divided by the total moles of the powder mixtures (Zn + graphite). A Au-coated (about 9 nm) Si(100) substrate was used to collect the product.

The as-synthesized product was analyzed by X-ray diffraction (XRD; Philips X'pert MRD diffractometer), scanning electron microscope (SEM, Hitachi S-4300 SE), and transmission electron microscopy (TEM). The photoluminescence (PL) measurements of the samples were carried out at 300 K using the 325 nm line of a He–Cd laser (KIMMON, ik3102 R-G) as an excitation source. The signal was detected by a cooled photomultiplier tube (ISA Jobin-Yvon R955) through a lock-in amplifier (Princeton Applied Research 5210). The Raman spectra were acquired by a Jasco Laser Raman Spectrophotometer NRS-3000 Series, with an excitation laser wavelength of 532 nm, at a power density of 2.9 $mW \cdot cm^{-2}$. XPS (VG Multilab ESCA 2000 system, UK) analysis was performed to analyze the elemental compositions, using a monochromatized Al Kα X-ray source ($h\nu = 1486.6$ eV).

3. RESULTS AND DISCUSSION

Figure 1(a) shows a top-view SEM image, revealing that large-scale production of the 1D structures was achieved. The enlarged SEM image shown in Figure 1(b) indicates that the surface of the 1D nanowire is relatively rough.

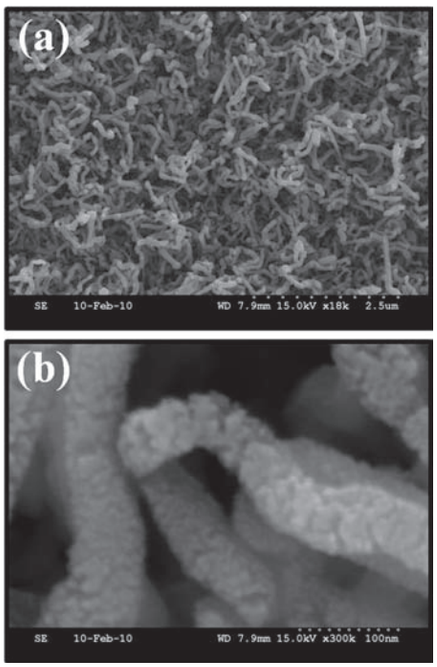

Figure 1. (a) Top-view SEM images of the nanowires. (b) Enlarged SEM image.

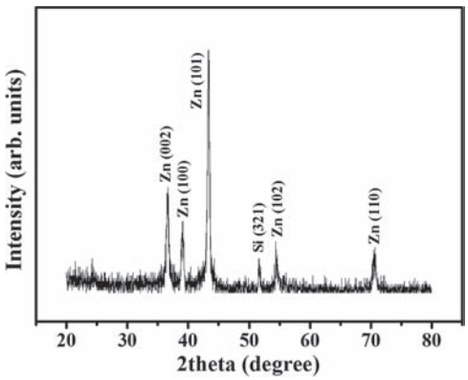

Figure 2. XRD pattern of the Zn nanowires.

Figure 2 shows an XRD spectrum of the product. Apart from Si-related peaks from the substrate, all recognizable diffraction peaks can be indexed to the hexagonal Zn with lattice constants $a = 2.665$ Å and $c = 4.947$ Å (JCPDS 04-0831).

A low magnification TEM image of a nanowire is shown in Figure 3(a), indicating that the nanowire has a serpent-like morphology. The diameter of the nanowire is estimated to be 50–65 nm. Figures 3(b) and (c) show a selected area electron diffraction (SAED) pattern and lattice-resolved TEM image, enlarging a squared region in Figure 3(a). The SAED pattern was recorded perpendicular to the rod axis, as it was indexed for the [010] axis of crystalline Zn. The diffraction spots, corresponding to the (001), (100), and (101) lattice planes of hexagonal Zn, can

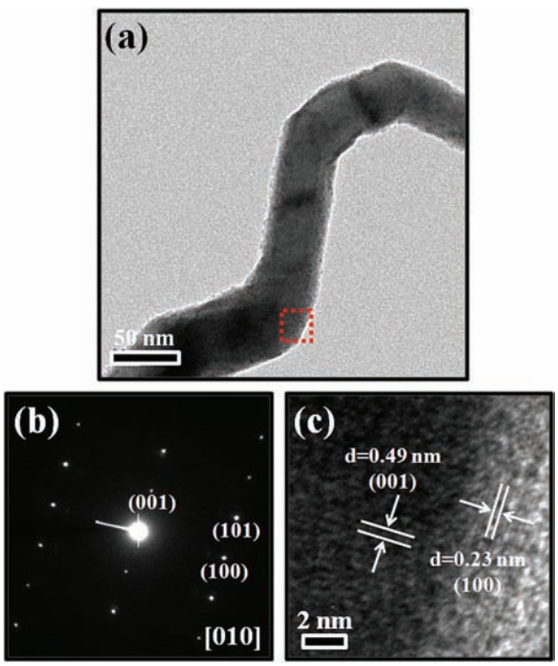

Figure 3. (a) TEM image of a Zn nanowire. (b) SAED pattern and (c) lattice-resolved TEM image from the squared region in (a).

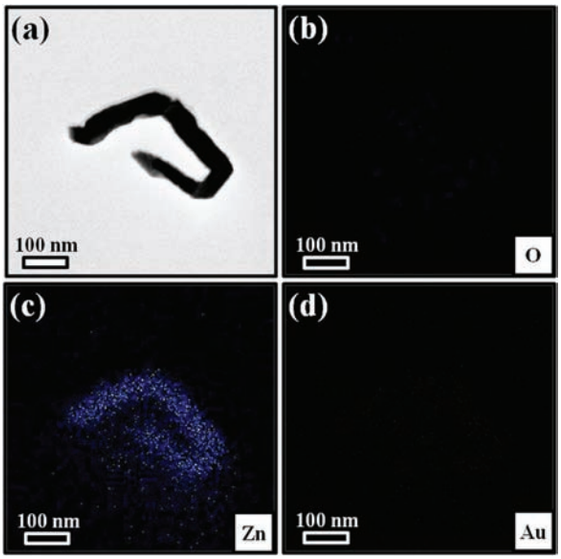

Figure 4. (a) Typical TEM image and EDX elemental maps of (b) O, (c) Zn, and (d) Au elements.

be observed. Also, in the lattice-resolved TEM image, the interplanar spacings are approximately 0.23 and 0.49 nm, corresponding to the (100) and (001) planes of hexagonal Zn.

The EDX measurements made of a typical nanowire indicate that the nanowire is mainly comprised of Zn elements (Fig. 4). Figure 4(a) is a typical TEM image and Figures 4(b)–(d) show the EDX elemental maps of O, Zn, and Au elements, respectively. Since the EDX elemental map does not explicitly reveal the presence of O elements (Fig. 4(b)), it is surmised that genuine hexagonal Zn nanowires, rather than ZnO, have been prepared. Owing to the absence of Au catalyst particles, the growth in the present study corresponds to the vapor-solid (VS) process.

In that case, during the evaporation process, Zn powders will be changed into Zn vapors, combining with Au films on the substrate surface. The addition of Zn lowers the melting point of Au, generating a liquid phase. Subsequently, solid Zn grows on the liquid phase surface, forming the Zn nanowires. Preliminary experiments revealed that the evaporation of Zn powders without graphite produced ZnO nanowires instead. Accordingly, it is evident that the graphite powders played a crucial role in fabricating the Zn nanowires. At the reaction temperature of 900 °C, the free energy of oxidation of solid Zn is calculated to be about − 239.034 kJ/mol, based on the following reaction: $Zn(s) + 1/2O_2(g) \rightarrow ZnO\ (s)$.[16] On the other hand, the free energy of oxidation of solid C is calculated to be

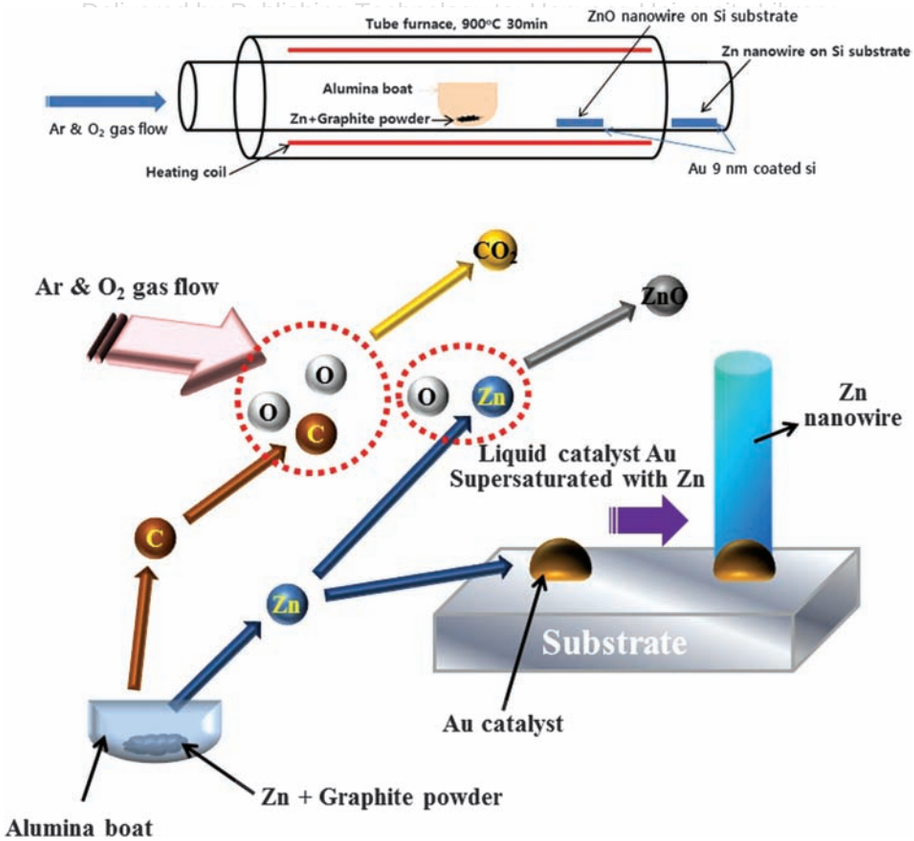

Figure 5. Schematic outline of the growth of Zn nanowires.

about − 396.208 kJ/mol, based on the following reaction: $C(s) + O_2(g) \rightarrow CO_2$ (g).[16]

Accordingly, considering the thermodynamics, graphite will be preferentially oxidized, with the oxidation of Zn being significantly suppressed. Following this, a significant amount of Zn will be oxidized, forming ZnO nanowires (Fig. 5). At this stage of the process, the oxygen will be considerably consumed. The unoxidized Zn will be deposited on the Si substrate as Zn nanowires with the assistance of Au catalysts. Accordingly, Zn nanowires will be formed preferentially in the deep position in the direction of gas flow. Based on the above observations, we have proposed the growth mechanisms for this process (Fig. 5).

Preliminary experiments indicated that the presence of the Au layer was crucial to the formation of Zn nanowires. However, the TEM investigation in the present study reveals that there are no Au-related nanoparticles at the tips of the nanowires. Accordingly, we surmise that the Au catalyst remains on the substrate at the bottom of the produced nanowires. The Zn–Au binary phase diagram certifies that the melting point of Zn will be decreased by the addition of Au. Since the addition of Au will induce less supercooling, the secondary growth from the stem rods will be suppressed. Instead, this situation will favor the formation of relatively thin 1D structures.

Figure 6(a) shows a Raman spectrum of the Zn nanowires synthesized in the present work, whereas Figure 6(b) shows that of ZnO nanowires, which were prepared in our laboratory. The spectrum of ZnO nanowires exhibits the typical Raman active modes, including A1(TO), E1(TO), E2(high), A1(LO), and E1(LO). On the other hand, the spectrum of Zn nanowires exhibits a prominent peak at around 570 cm^{-1}, which is considerable higher than the E2 peak. Similar features have been reported in previous reports,[17, 18] and are caused by the presence of a depletion region near the grain boundaries of Zn-rich microscrystalline ZnO particles. This may indicate that the Zn nanowires have a Zn-rich ZnO_x structure.

Figures 7(a) and (b) show the raw-scan XPS spectra of Zn nanowires and ZnO nanowires, respectively. Although the theoretical atomic percentage of oxygen in ZnO will be 50%, it is found that the surface of the ZnO nanowires have O and Zn atomic concentrations of 67.3 and 32.7%, respectively (Fig. 7(b)). It is expected that the ZnO surface will be oxygen-rich due to the presence of ambient air.

On the other hand, the surface of the Zn nanowires exhibits O and Zn atomic concentrations of 55.0 and 45.0%, respectively (Fig. 7(a)). Considering that the bulk oxygen atomic concentration of ZnO should be 50%, the surface of ZnO will contain more oxygen that the bulk ZnO. Similarly, the surface of the Zn nanowires will contain a significant amount of oxygen. By comparing Figures 7(a) with (b), we observe that the oxygen-richness of the surface of the Zn nanowires is clearly smaller than that of the ZnO nanowires. We surmise that the difference in original bulk composition results in the different surface compositions.

Figure 8(a) shows the PL spectrum of the ZnO nanowires. It is apparent that the spectrum is comprised of green emission centered around 2.4 eV, and UV emission centered around 3.2 eV. The green emission peaked at 2.4 eV is usually attributed to oxygen vacancies (V_O^+). For comparison, Figure 8(b) shows the PL spectrum of the Zn nanowires. The spectrum also exhibits the green emission

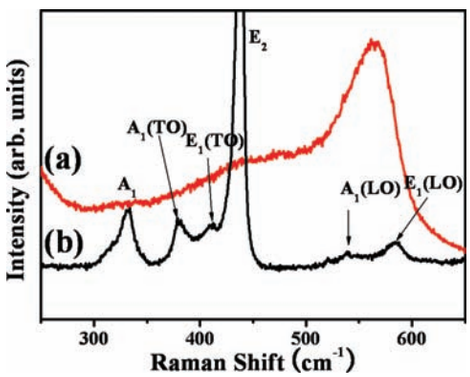

Figure 6. Raman spectra of (a) Zn nanowires and (b) ZnO nanowires.

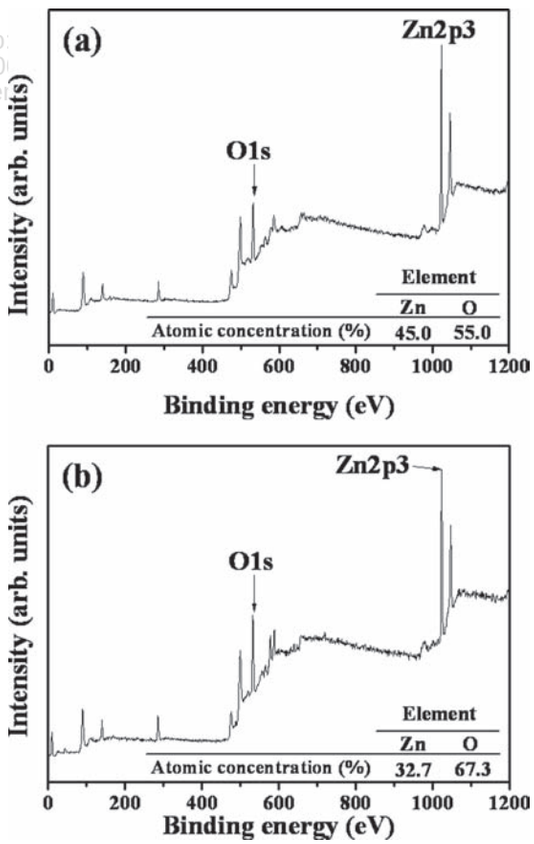

Figure 7. Raw-scan XPS spectra of (a) Zn nanowires and (b) ZnO nanowires.

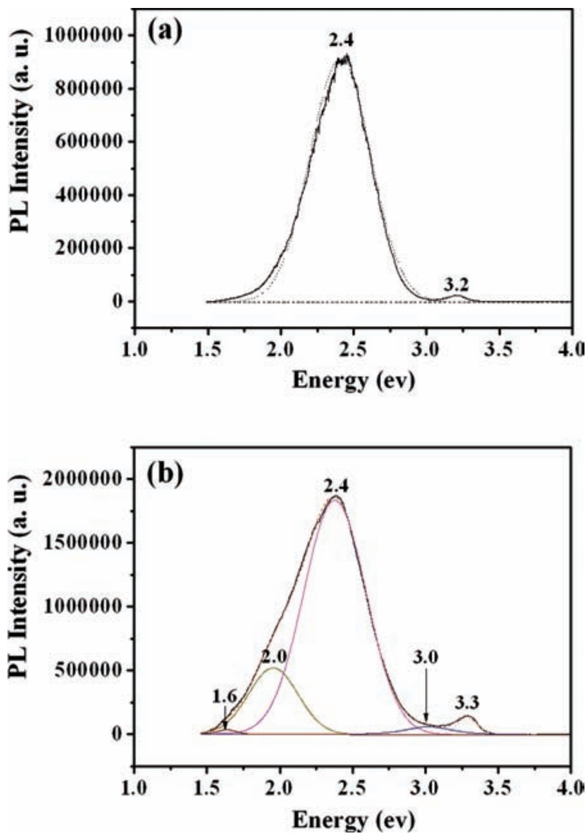

Figure 8. PL spectra of (a) ZnO nanowires and (b) Zn nanowires.

($\sim$2.4 eV) and the UV emission ($\sim$3.3 eV). Based on the presence of the green emission, we suppose that the Zn nanowires include a significant amount of ZnO_x-related structures. In fact, TEM and XPS analyses reveal in a complementary manner that the ZnO_x structure is concentrated on the surface of the Zn nanowires. In addition, Figure 8(b) exhibits a 2.0 eV-peaked emission in the orange region and a 1.6 eV-peaked one in the red region. The red emission is ascribed to oxygen vacancies (V_O).[19] We surmise that the red emission is related to the presence of a Zn-rich ZnO phase in the Zn nanowires. Also, it is possible that the 3.0 eV-peak from the Zn nanowires originates from Zn vacancies.[19]

4. CONCLUSION

We have synthesized Zn nanowires by heating a mixture of Zn and graphite powders at 900 °C. TEM investigation reveals that the nanowire has a serpent-like morphology with a diameter in the range of 50–65 nm. XRD, SAED, and lattice-resolved TEM images coincidentally indicate that the nanowires are crystalline with a hexagonal Zn phase. EDX analysis reveals that the nanowire is mainly comprised of Zn elements. Due to the absence of metal catalyst particles, the growth is determined to be mainly dominated by the VS process. Raman spectra of the Zn nanowires exhibit a prominent peak at around 570 cm^{-1}, implying the presence of a Zn-rich ZnO_x structure. XPS spectra reveal that the oxygen-richness of the surface of Zn nanowires is clearly smaller than that of ZnO nanowires. Gaussian convolution analysis indicates that the PL spectrum of Zn nanowires is comprised of 1.6, 2.0, 2.4, 3.0, and 3.3 eV-centered peaks.

Acknowledgment: This work was supported by the National Research Foundation of Korea (NRF) grant funded by the Korea government (MEST) (No. NRF-2013R1A2A2A01068438).

References and Notes

1. M. Ahmadi, K. Mirabbaszadeh, and M. Ketabchi, *Electron Mater. Lett.* 9, 729 (**2013**).
2. T. Sahoo, L.-W. Jang, D.-W. Jeon, Y.-T. Yu, and I.-H. Lee, *Electron Mater. Lett.* 9, 715 (**2013**).
3. H. Yoon, G. Nam, H. Park, J.-S. Son, and J.-Y. Leem, *Electron Mater. Lett.* 9, 545 (**2013**).
4. K. Seo, M. Suh, and S. Ju, *Electron Mater. Lett.* 9, 273 (**2013**).
5. R. Kuar, M. C. Mishra, B. K. Sharma, V. Vyas, and G. Sharma, *Electron. Mater. Lett.* 9, 19 (**2013**).
6. H.-W. Cui, D.-S. Li, and Q. Fan, *Electron. Mater. Lett.* 9, 1 (**2013**).
7. X. W. Wang, G. T. Fei, K. Zheng, Z. Jin, and L. D. Zhang, *Appl. Phys. Lett.* 88, 173114 (**2006**).
8. Y. Kondo and K. Takayanagi, *Science* 289, 606 (**2000**).
9. B. L. Wang, S. Y. Yin, G. Wang, and A. Buldum, *Phys. Rev. Lett.* 86, 2046 (**2001**).
10. J. Mallet, K. Y. Zhang, C. L. Chien, T. S. Eagleton, and P. C. Searson, *Appl. Phys. Lett.* 84, 3900 (**2004**).
11. S.-S. Chang, S. O. Yoon, H. J. Park, and A. Sakai, *Mater. Lett.* 53, 432 (**2002**).
12. S. R. C. Vivekchand, G. Gundiah, A. Govindaraj, and C. N. R. Rao, *Adv. Mater.* 16, 1842 (**2004**).
13. M. Kast, P. Schroeder, Y. J. Hyun, P. Pongratz, and H. Bruckl, *Nano Lett.* 7, 2540 (**2007**).
14. X. W. Wang, G. T. Fei, K. Zheng, Z. Jin, and L. D. Zhang, *Appl. Phys. Lett.* 88, 173114 (**2006**).
15. J.-G. Wang, M.-L. Tian, N. Kumar, and T. E. Mallouk, *Nano Lett.* 5, 1247 (**2005**).
16. I. Barin, Thermochemical Data of Pure Substances, Third Edition, Wiley VCH, Weinheim, Germany (**1997**).
17. W.-B. Cai and D. A. Scherson, *J. Electrochem. Soc.* 150, B217 (**2003**).
18. M. Tzolov, N. Tzenov, D. Dimova-Malinovska, M. Kalitzova, C. Pizzuto, G. Vitali, G. Zollo, and I. Ivanov, *Thin Solid Films* 379, 28 (**2000**).
19. B. Lin, Z. Fu, Y. Jia, and G. Liao, *J. Electrochem. Soc.* 148, G110 (**2001**).

Received: 23 January 2014. Accepted: 26 March 2014.